The Molecular Tweezer CLR01 Stabilizes a Disordered Protein-Protein Interface

David Bier[a,b], Sumit Mittal[c,#], Kenny Bravo-Rodriguez[c,#],Andrea Sowislok[b,#], Xavier Guillory[a,b], Jeroen Briels[a,b], Christian Heid[b], Maria Bartel[a], Burkhard Wettig[b], Luc Brunsveld[a], Elsa Sanchez-Garcia[c,*], Thomas Schrader[b,*], Christian Ottmann[a,b,*]

[a] Laboratory of Chemical Biology, Department of Biomedical Engineering and Institute for Complex Molecular Systems, Eindhoven University of Technology, Den Dolech 2, 5612 AZ Eindhoven, The Netherlands.

[b] Department of Chemistry, University of Duisburg-Essen, Universitätsstrasse 7, 45117 Essen, Germany.

[c] Max-Planck-Institut für Kohlenforschung, Kaiser-Wilhelm-Platz 1, 45470 Mülheim an der Ruhr, Germany.

[#] These authors contributed equally.

[*] Corresponding author

Supplementary Material

X-ray crystallography table..... S2

Supplementary figures crystallography S3

Investigation of model systems in aqueous buffer..... S7

Protein expression and purification S11

Extended computational details S11

References..... S23

Table S1: **Data collection and refinement statistics (molecular replacement)**

	14-3-3ζ/Cdc25C (5M35)	14-3-3ζ/Cdc25C (38mer)/CLR01 (5M36)	14-3-3ζ/Cdc25C (20mer)/CLR01 (5M37)
Data collection			
Wavelength (Å)	0.99983	1.00000	0.97793
Space group	$P2_12_12_1$ (19)	$P2_12_12_1$ (19)	$P2_12_12_1$ (19)
Cell dimensions			
a, *b*, *c* (Å)	72.22, 104.07, 114.45	71.52, 102.36, 112.82	71.17, 88.21, 112.59
α, β, γ (°)	90.00, 90.00, 90.00	90.00, 90.00, 90.00	90.00, 90.00, 90.00
Resolution (Å)	44.85-2.38(2.52-2.38)	46.61-2.45(2.60-2.45)	49.70-2.35 (2.60-2.35)
$CC_{1/2}$ /R_{pim}	100(75.7)/0.026(0.28)	100(95.9)/0.036(0.51)	99.9(97.0)/0.028(0.54)
I / σI	16.76(3.11)	26.68(3.10)	20.56(3.61)
Completeness (%)	99.70(99.90)	99.90(99.80)	99.60(99.60)
Redundancy	6.40(6.78)	13.06(13.01)	13.00(12.76)
Refinement			
Resolution (Å)	44.85-2.38(2.52-2.38)	46.61-2.45(2.60-2.45)	49.70-2.35 (2.60-2-35)
No. reflections	33123	31100	30093
R_{work} / R_{free}	0.2332/0.2820 (0.334/0.436)	0.2365/0.2726(0.4312/0.4670)	0.2320/0.2820(0.4319/0.4556)
No. atoms			
Protein	1799/1743	1725/1749	1806/1758
Ligand/ion	82/54	153/71/208/18	134/130/208/18
Water	94	67	162
Average *B*-factors			
Protein	56.56/56.05	75.98/76.35	59.91/66.76
Ligand/ion	72.23/91.27	123.10//116.76/131.63/85.18	88.31/76.59/93.41/56.16
Water	58.32	72.59	59.96
R.m.s. deviations			
Bond lengths (Å)	0.021	0.025	0.025
Bond angles (°)	1.935	1.420	1.350
Ramachandran			
Preferred (%)	95.58	97.05	96.63
Allowed (%)	4.42	2.95	3.37
Outliers (%)	0.0	0.0	0.0

*Values in parentheses are for the highest-resolution shell.

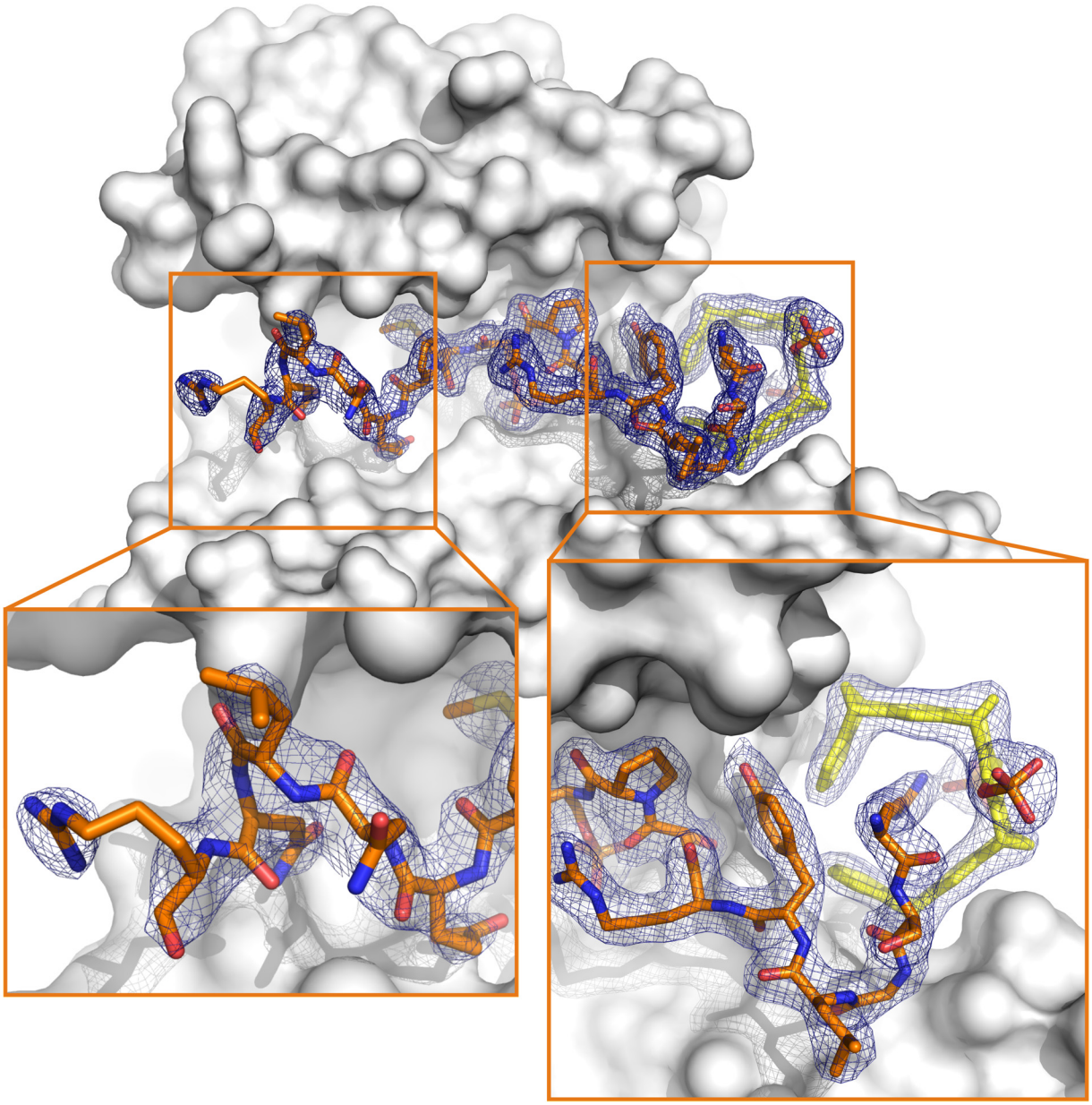

Figure S1. Crystal structure of Cdc25CpS216 (20mer, orange sticks) in complex with 14-3-3ζ (white surface). Depicted is the final $2F_o$-F_c electron density map contoured at 2.5σ (blue mesh) in the upper panel as an overview showing the entire amphipathic groove and in the lower panel as close-up views of the C-terminal (left) and N-terminal (right) part of the Cdc25CpS216 peptide.

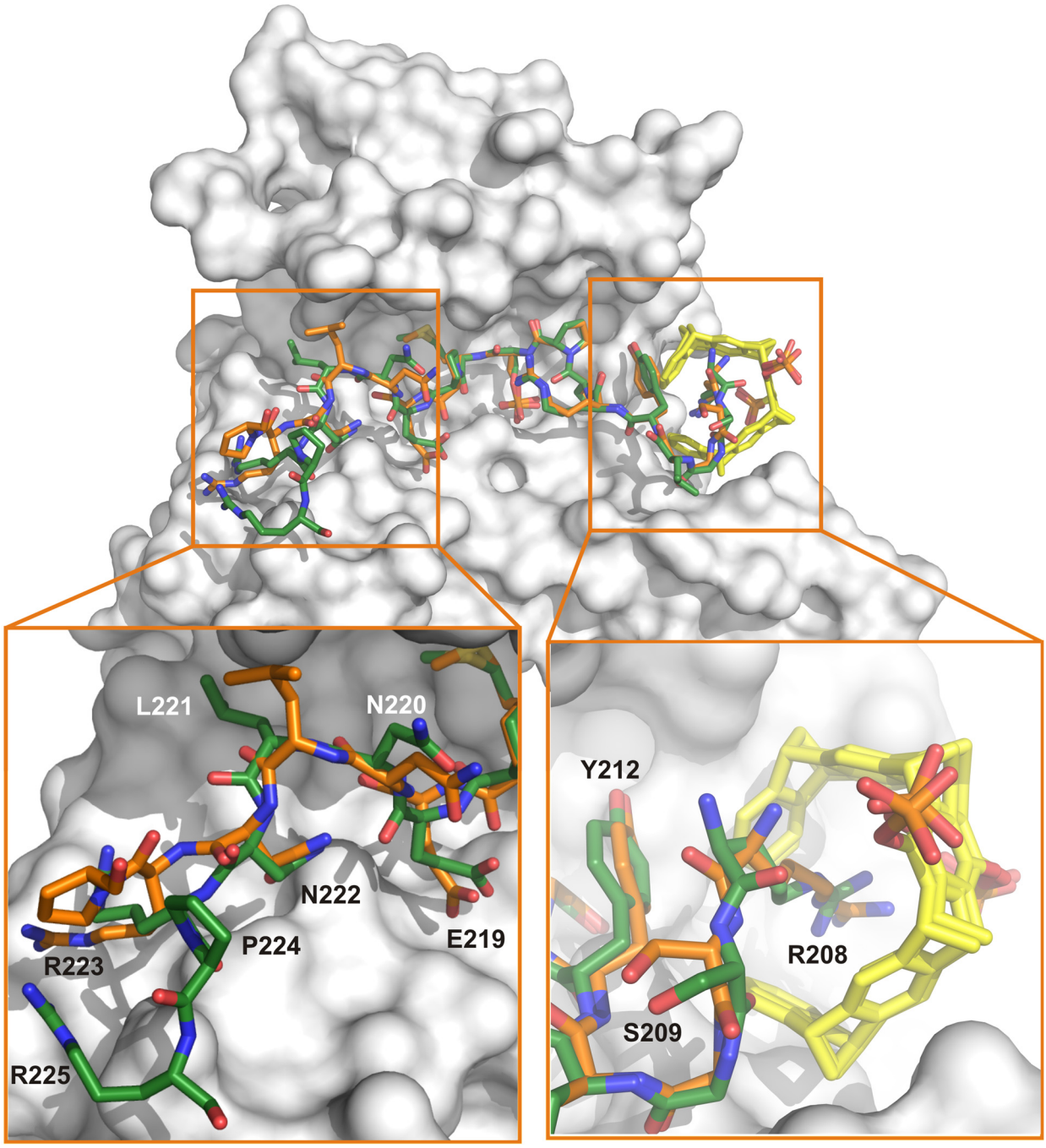

Figure S2. Overlay of the crystal structures of Cdc25CpS216 (20mer, orange sticks) and Cdc25CpS216 (38mer, green sticks) in complex with 14-3-3ζ (white surface) and CLR01 (yellow sticks).

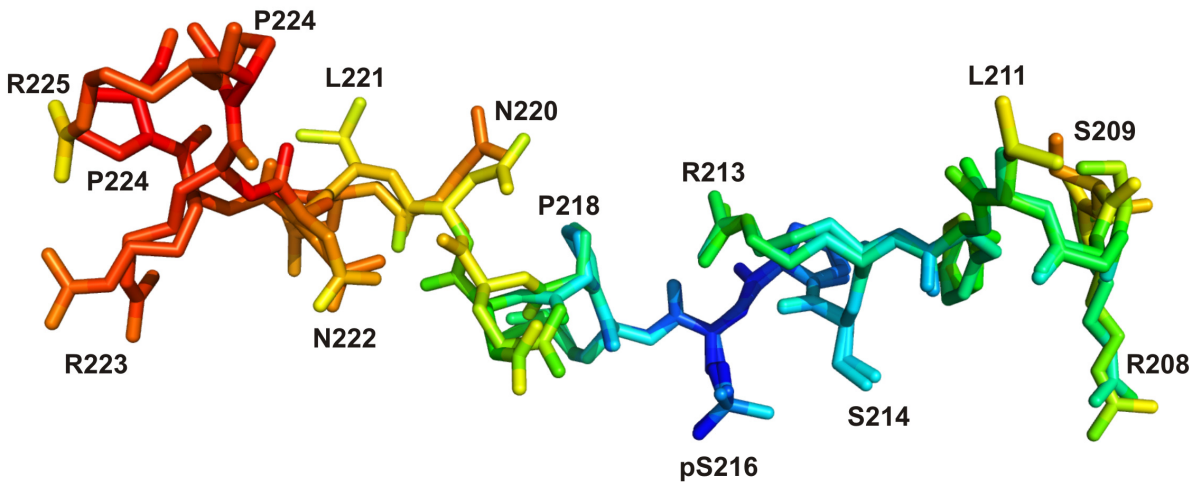

Figure S3. Superimposition of the 20- and 38mer Cdc25CpS216 peptide colored by B factor. While the N-terminal part is rather rigid, the C-terminal part shows increased flexibility.

Investigation of model systems in aqueous buffer

To gain more functional information, we investigated if $R208_{Cdc25C}$ is also accommodated in the tweezer's cavity in free aqueous solution. To this end, the C-terminal part of the truncated Cdc25CpS216 peptide (S207-L211/S207-Y212) was titrated with CLR01 in the same aqueous buffer as used for the fluorescence polarization experiment. As expected, the tweezer fluorescence was efficiently quenched, indicating inclusion inside the tweezer cavity. Binding isotherms were obtained whose curve-fitting by nonlinear regression documented a 1:1 complex stoichiometry and a K_d of around 30µM, even stronger than previous titrations of arginine-containing peptides. In NMR titrations substantial upfield shifts occurred in the methylene proton signals of $R208_{Cdc25C}$, which reached maximum Δδ values of more than 2 ppm on saturation. This is proof of the threading mechanism, bringing the arginine's side chain close to the anisotropy of the convergent aromatic rings.

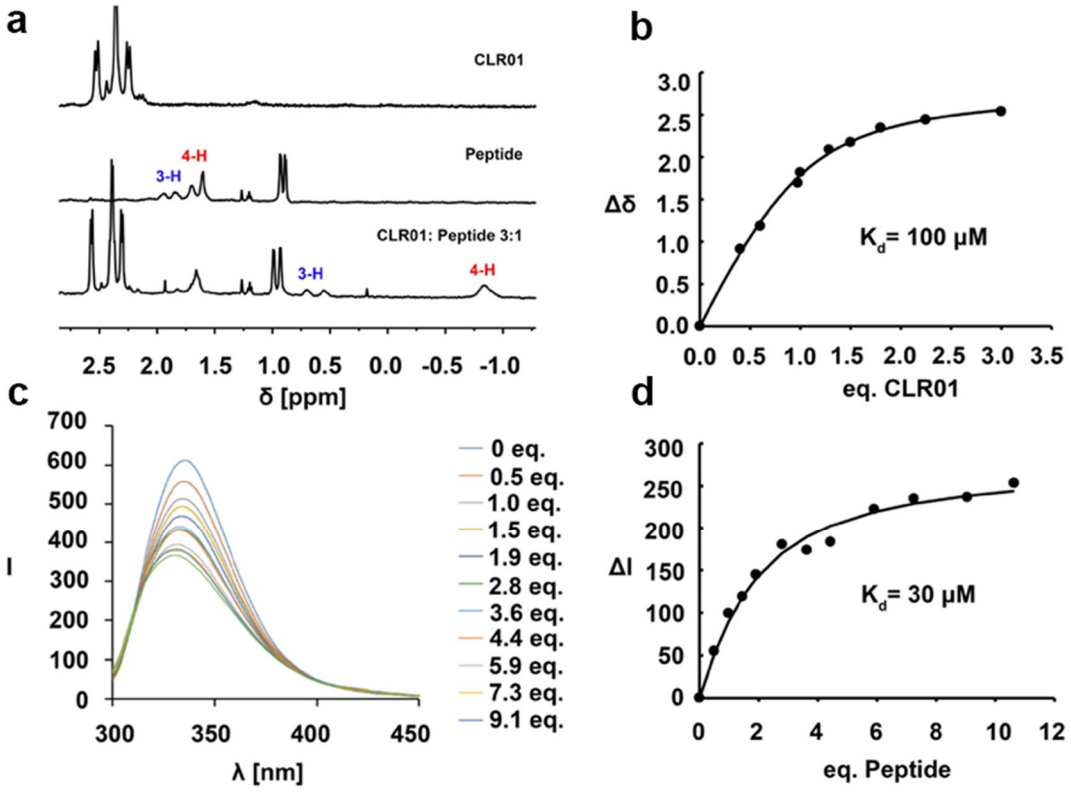

Figure S4. Titration experiments between an N-terminal Cdc25 model and CLR01. a) ^{1}H NMR spectra of CLR01, the free model peptide S**R**SGLY (S207-Y212 region of the Cdc25CpS216 peptide) and their 3:1 complex. Note the strongly negative chemical shift changes of arginine's side chain protons indicative of its insertion into the tweezer cavity. b) Binding isotherm of the full NMR titration experiment at 0.5 mM peptide concentration). c) Fluorescent spectra of CLR01 in the presence of increasing peptide concentrations. Note the significant quenching of the tweezers fluorescence emission. d) Resulting binding isotherm at 20 µM tweezers concentration.

No direct interaction between CLR01 and fluorescence label

In order to rule out a potential interaction between CLR01 and the fluorescence label (Fluorescein), a very short NMR titration was carried out between the isolated compounds, and potential chemical shift changes in the aromatic regions of both compounds were monitored. In case of a fluorescein inclusion, strong upfield shifts should occur, whereas an external π,π-interaction would furnish modest upfield and/or downfield shifts.

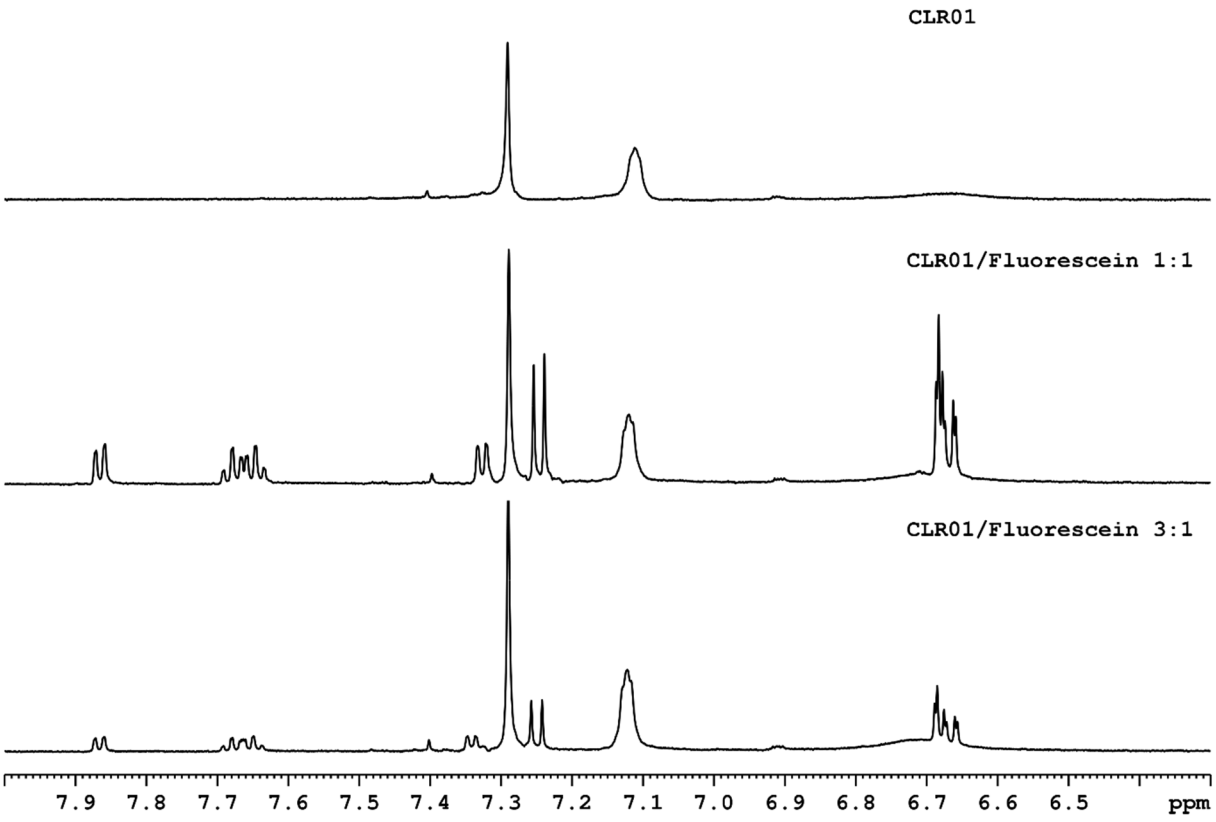

Figure S5a. NMR titration (600 MHz) of molecular tweezers (CLR01, 2 mM) with fluorescein in 10 mM phosphate buffer at pH = 7.4. The superimposition of NMR spectra for pure tweezer, its 1:1 and 3:1 complex with fluorescein documents that no chemical shift changes occur in the aromatic region, neither in the tweezer nor the fluorescent dye molecule. This rules out a potential direct interaction of the extended aromatic moieties. Likewise, no shift changes are observed in all other signals of host and guest ($\Delta\delta < 0.05$ ppm).

As independent confirmation, we also titrated the tweezers with fluoresceine and measured the evolved heat changes by microcalorimetry. However, in the course of this ITC titration, no heat changes occurred (< 0.05 µcal/s). We conclude, that even at millimolar concentrations, enthalpy gains remain very small - as if buffer was titrated into buffer. Thus, no evidence for a direct tweezer/fluorophore interaction was found with ITC.

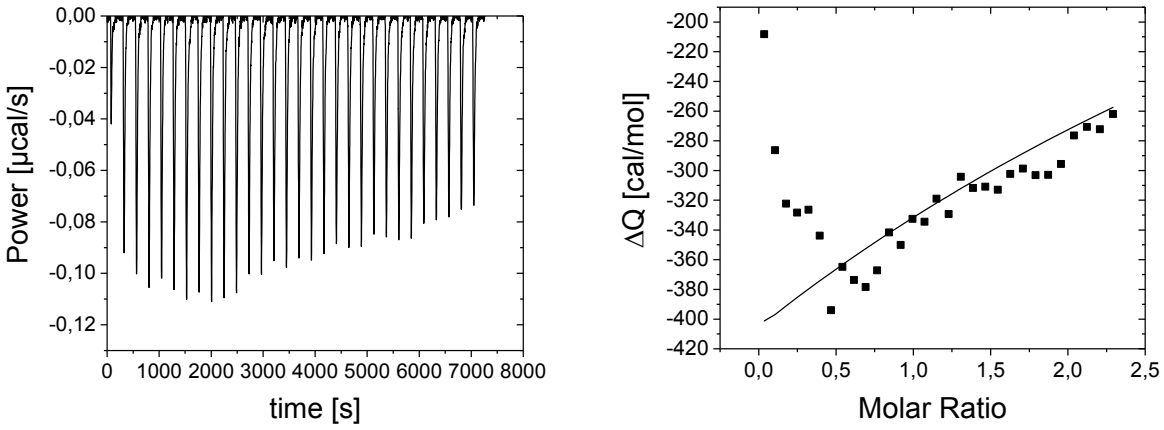

Figure S5b. ITC titration between CLR01 and fluorescein: no appreciable heat changes occur.

Conditions

- Fluorescein c = 0.1 mmol/L in cell
- CLR01 c = 1 mmol/L in syringe
- One-site model
- Solvent: Phosphate buffer 10 mM pH = 7.4
- Molar ratio → up tp 2.3 eqs. of tweezer

Determination of CLR01's *p*k_a value.

For the determination of the second P-OH *p*k_a value of CLR01, the tetra sodium salt of the molecular tweezer was dissolved in $H_2O_{(bidest.)}$ (*p*H = 7.35) with a concentration of $c_{(CLR01)}$ = 0.01 M. A volume of 1 mL of the tweezer solution was subsequently titrated with HCl (c = 0.001 M) in 0.5 ml steps at room temperature. The corresponding pH values were measured using a SevenGo^{TM} *p*H meter SG2 METTLER TOLEDO InLab® pH combination electrode with XEROLYT® polymer electrolyte.

Plotting the values lead to the black curve in Fig. S6. At half equivalence volume the corresponding pH indicates a pKa value of ~7.5. The first derivative (red curve) was calculated using the formula $y = |(pH_{(n+1)}-pH_{(n)})/(V_{(n+1)}-V_{(n)})|$ and plotted over the average volumes $V_{(av)} = (V_{(n+1)}-V_{(n)}/2)$. The first derivate also indicates a half equivalence volume of 1.625 mL with the corresponding *p*k_a value of 7.4. Both values are in good agreement.

The obtained *p*k_a value matches perfectly with the second *p*k_a value of phosphoric acid. The result indicates a doubly monoprotonated phosphate species of the molecular tweezer at physiologic conditions.

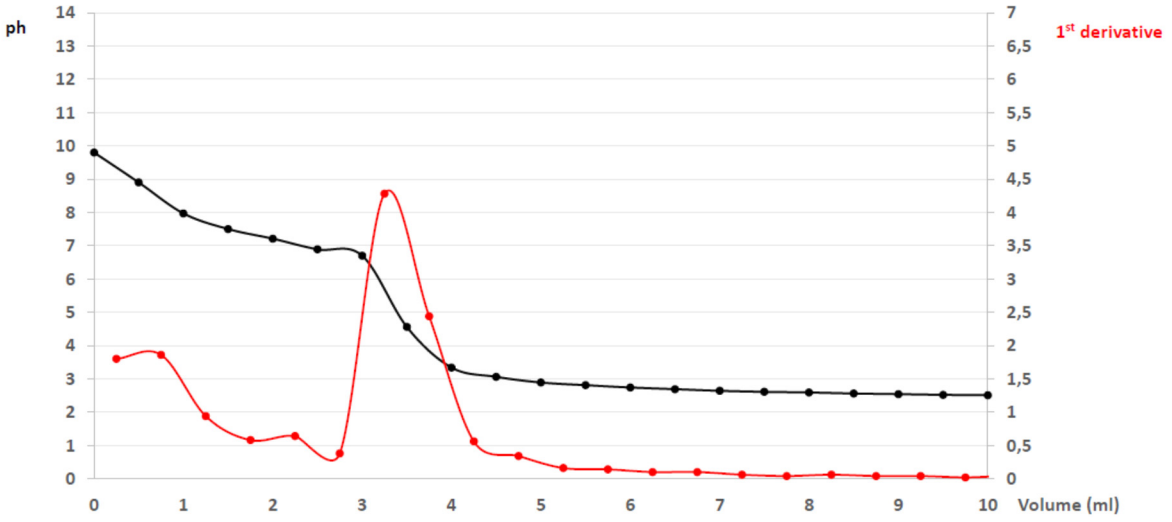

Figure S6. pKs determination of the second POH deprotonation step in CLR01. Black curve: potentiometric titration; red curve: first derivative.

Fluorescence titrations

Sample Preparation. First, a tweezer solution was prepared in PBS buffer at a concentration of $2.12 \cdot 10^{-5}$ M. Subsequently, the peptide standard solution was prepared from the tweezer solution. Therefore, the peptide was weighed precisely and added to the tweezer solution, so that its concentration was 7.50 x 10^{-4} M. Thus, the peptide standard solution contained a tweezer:peptide ratio of ~ 1:35.

Procedure. 700 µL of the tweezer solution were placed in the sample cell and a fluorescence spectrum was measured. The λ_{max} (maximum intensity) and the intensity at this wavelength were determined. Subsequently, the peptide standard solution was titrated to the tweezer solution: up to a total volume of 800 µL, the peptide solution was added in 10 µL increments; 30 s after each addition a fluorescence spectrum was recorded and the intensity at λ_{max} determined. Up to a total volume of 1000 µL the titration was continued in 40 µL steps. Based on the changes in intensity at λ_{max} (binding curve), a non-linear regression was used to determine the corresponding K_a value.

Isothermal titration calorimetry

Sample Preparation. The protein standard solutions were prepared by carefully pipetting the appropriate volumes from 14-3-3 solution at a concentration of 1.628 mM and, for PPI stabilization experiment, from a CLR01 tweezer solution at a concentration of 2.0 mM, both in ITC buffer [25 mM Hepes, pH 7.4, 100 mM NaCl, 10 mM $MgCl_2$, 0.5 mM Tris-(2-carboxyethyl)-phosphin]. The peptide standard solution was prepared by precisely weighing the dry peptide on a precision balance and dissolving it with ITC buffer to reach a concentration of 1.26 mM.

Procedure. The ITC measurements were performed on a Malvern MicroCal iTC200. The cell contained 0.1 mM 14-3-3ζ and the syringe contained a peptide solution at 1.26 mM, both in ITC buffer. For the PPI stabilization experiments, the cell contained 0.1 mM 14-3-3 and either 0.25 mM or 1.50 mM CLR01. The experiments were performed in triplicates and consisted of a series of 18 2-µL titrations performed at 25 °C (reference power, 5 µCal/s; initial delay, 180 s; stirring speed, 750 rpm; spacing, 200 s).

NMR titrations

Sample Preparation. First a peptide solution was prepared in a PBS buffer at a concentration of 0.5 mM. From the peptide solution the tweezer standard solution was prepared, at a concentration of 1.5 mM. Thus, the tweezer standard solution contained a peptide/tweezer ratio of 1:3.

Procedure. 600 µL of the tweezer standard solution were placed in an NMR-tube and the ^{1}H NMR spectrum was recorded. Subsequently, this tweezer standard solution was diluted in 50 µl steps with peptide solution up to a total volume of 1.00 mL and at each step a ^{1}H NMR spectrum was recorded. Up to a total volume of 1.60 mL, the titration was continued in 100 µL steps. As a reference, a spectrum of the pure peptide (0.5 mM) in PBS buffer was recorded. From the chemical shift changes a binding curve was generated and the K_a value was determined by nonlinear regression.

Protein expression and purification.

The pProEx HTb plasmid containing the 14-3-3ζ (aa 1-230) cDNA were transformed into *E.coli* cells (strain: Rosetta (DE3)). For protein expression, 2.5 L Terrific Broth media was inoculated with an overnight pre-culture, followed by incubation at 37 °C until the OD_{600} value reached 0.7. The protein expression was started by addition of 0.4 mM IPTG and continued incubation of culture for 15 h at 20 °C. After cell harvesting, the cell pellet was resuspended in lysis buffer (50 mM TRIS (pH 8.0), 500 mM NaCl, 2 mM PMSF and 2 mM β-mercaptoethanol). After cell disruption and centrifugation steps (65.000 rcf, 8 °C for 45 min), the 14-3-3ζ protein was isolated from the lysate by affinity chromatography (Ni-NTA beads, Qiagen). For removing of the His-tag, the protein was incubated with Tobacco Etch Virus (TEV) protease in a ratio of 1:0.05 mg, followed by SDS PAGE purity control and size exclusion chromatography (SEC) (50 mM HEPES (pH 7.5), 100 mM NaCl, 2 mM $MgCl_2$; Column: 26/60 Sephacryl S200, (GE Healthcare) The protein was concentrated to 50-100 mg/ml and 50 µL aliquots stored at −80 °C.

Extended computational details

For the simulations, the initial coordinates were taken from the crystal structure of the ternary complex reported here. The residues missing in the crystal structure were included using Modeller 9.10[1]. Ser216 of Cdc25CpS216 was kept phosphorylated as found in the crystal structure. The peptide-protein complex has 20 lysine residues in the 14-3-3ζ protein and 15 arginine residues (11 in 14-3-3ζ and four in Cdc25CpS216). All possible complexes (1:1:1 ratio) were studied, resulting in 35 ternary complexes. Each complex was first energy minimized using CHARMM[2-3]. The system was solvated in TIP3P water[4] and neutralized by adding Na^+ ions. This was followed by 500 ps NVT molecular dynamics simulations with protein and tweezer atoms fixed in their initial coordinates. Afterwards the systems were subjected to 500 ps NPT dynamics with only the backbone of the proteins fixed. Finally, 75 ns production MD simulations were performed for each complex. All MD simulations were performed using the NAMD 2.9 program[5] and the CHARMM27 force field[6-7]. A time step of 2 fs was used in all simulations and the hydrogen bonds were constrained using SHAKE[8]. The temperature was maintained at 300 K using the Langevin thermostat[9]. The Particle-mesh Ewald (PME) algorithm was used to handle the electrostatic interactions[10]. Ten inclusion complexes were not conserved due to steric clashes (Figs. S9). The remaining systems were investigated using QM/MM calculations.

The QM/MM optimizations were performed at the B3LYP-D3/def2-SVP//CHARMM27 level of theory using ChemShell v3.5[11]. For each complex three snapshots were selected. An electrostatic embedding scheme[12] was employed together with a charge shift scheme [13-14]. The active region consisted of a ~ 3000 atoms sphere centered on the nitrogen atom of the lateral chain of lysine (NZ) or on one of the NH2 groups of the lateral chain of arginine. The entire tweezer molecule together with part of the lysine or arginine side chain was chosen as the QM region (Fig. S7). All atoms within the active region were allowed to freely move in each optimization step.

The free energies of binding of CLR01 to the most favored lysine and arginine residues were computed via the alchemical transformation pathway[15]. The alchemical free energy perturbation (FEP) calculations involved the following simulations:

The free energy for the reversible decoupling of CLR01 from the lysine and arginine residues in

the protein – peptide complex was determined using the alchemical transformation pathway. A snapshot chosen from QM/MM calculations was the starting structure representing the binding of CLR01 to a particular lysine or arginine residue. The system formed by CLR01, 14-3-3ζ and Cdc25CpS216 was solvated with TIP3P water in a cubic box with a cell length of 100 Å.

The alchemical transformation was performed bidirectionally, creating and annihilating the CLR01 molecules, using 100 windows with 100,000 equilibration steps (0.1 ns) and data-collection over 900,000 molecular-dynamics steps (0.9 ns) for each window with a time step of 1 fs, resulting in a total simulated time of 100 ns. To ensure that CLR01 does not wander off when decoupled from the binding site, positional and orientation restraints were applied. For the restraints, 3 sites (atoms) were chosen in the ligand and 3 sites in the protein or peptide. Restraints were defined as collective variables during the simulation and the contribution of these collective variables was determined via thermodynamic-integration simulations by decreasing the force constant of the associated harmonic potential from its nominal value to zero in a stepwise manner. An additional restraint involving the RMSD value of CLR01 was applied for keeping CLR01 in its native conformation. In total, 7 geometric restraints were applied when CLR01 is in the binding site. The evaluation of the contribution from the restraints was done using 100 windows of the same width. Each window was equilibrated for 100,000 molecular-dynamics steps, followed by 900,000 data-collection steps. The total simulation time per restraint was 100 ns (time step 1 fs).

Similar alchemical simulations were performed for the CLR01 molecule solvated in a 100 X 100 X 100 $Å^3$ water box to complete the alchemical transformation cycle. Only RMSD restraints were applied to control the structural flexibility. The ParseFEP plugin of VMD was used to monitor the convergence of the alchemical transformations and to obtain the maximum-likelihood Benett-acceptance-ratio (BAR) estimator of the free energy by combining bidirectional simulations [16-17].

Additionally, two sets of umbrella sampling (US) simulations[18] were performed to investigate the effect of the tweezer on the binding of Cdc25C to 14-3-3ζ. The reaction coordinate was taken as the distance between the centers of mass of 14-3-3ζ and the Cdc25CpS216 – CLR01 complex. The reaction coordinate was divided into 48 windows with a separation of 1 Å. In order to generate the initial coordinates for the windows, a steered MD (SMD) simulation was performed in which the position of 14-3-3ζ remained constrained while the peptide alone and the peptide plus tweezer were moved away from 14-3-3ζ. The SMDs were done in the constant velocity regime. The force constant used was 7 kcal/mol/$Å^2$ and the velocity was 0.0005 Å/timestep. Prior to the US simulations, NVT simulations with 14-3-3ζ and Cdc25CpS216 or Cdc25CpS216-CLR01 fixed to their initial coordinates were done to properly equilibrate the solvent. During the umbrella sampling calculations each window was simulated for 7 ns for a total of 336 ns simulation time. The time step used was 1 fs. 14-3-3ζ was constrained in all cases with a harmonic potential restraining the movement of its center of mass and its rotations with force constants of 100 kcal/mol/$Å^2$ and 100 kcal/mol/degree^2, respectively. The distance between the centers of mass was restrained with a harmonic potential with a force constant of 10 kcal/mol/$Å^2$.

An additional set of US simulations was performed to estimate the effect of several CLR01 molecules bound to 14-3-3ζ (K187, K212, K139, K11, R18, R60, R80) and Cdc25CpS216 (R208, R213). The selection criteria for these positions were the QM energies (QM/MM calculations) or the close vicinity to the contact region between Cdc25CpS216 and 14-3-3ζ. The simulations details are the same as mentioned above except that a) the reaction coordinate was defined as the distance between the centers of mass of 14-3-3ζ and the Cdc25CpS216 – 2 $CLR01_{R208, R213}$ complex, 2) the

simulation time for each of the 48 windows was increased to 8 ns for better convergence.

In all US simulations, the first nanosecond of each window was discarded to account for the equilibration of the system. The simulation data for the remaining 7 ns (6 ns for 14-3-3ζ - Cdc25CpS216) was divided into 14 (12 for 14-3-3ζ - Cdc25CpS216) equal parts to check the convergence of the PMF (Fig. S10).

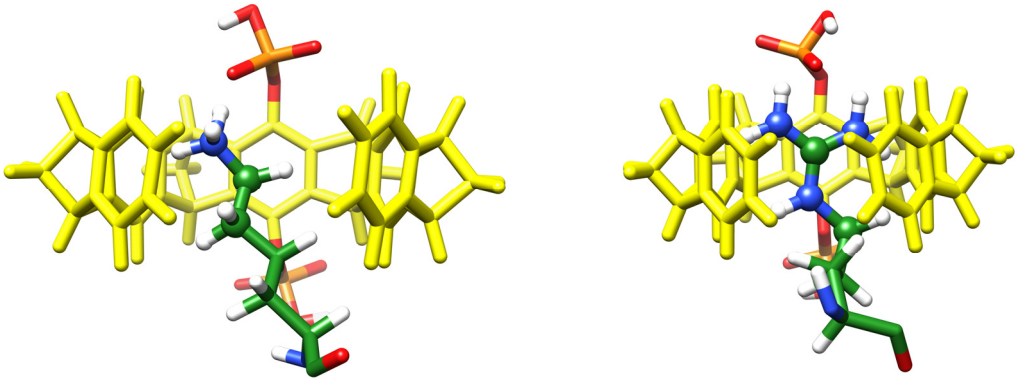

Figure S7. The QM regions included all atoms of the tweezers and the atoms of the side chain of lysine or arginine shown as spheres.

Hydrophobic collapse

A hydrophobic collapse was observed during the MD simulations. When the tweezer binds $R208_{Cdc25C}$, the nearby residue $R213_{Cdc25C}$ comes closer to the phosphate group of $S216_{Cdc25C}$, thus increasing the intramolecular interactions in the peptide (Fig. S11). Subsequently, the central hydrophobic residues of Cdc25CpS216, namely M217, P218, and L221, which are initially apart, come together as the simulations progress. This hydrophobic collapse is further enhanced by the interaction of nearby hydrophobic residues of the 14-3-3ζ protein (L168, L172, L216, L220 and I217) that come in contact with the hydrophobic cluster formed by M217, P218, and L221 of Cdc25CpS216. Leucine and isoleucine residues are reported to be crucial for binding of other peptides to 14-3-3ζ proteins.[19,20] This behavior of hydrophobic residues was not observed during the MD simulations in the absence of CLR01 as well as during most of the MD simulations where CLR01 interacts with other sterically available lysine or arginine residues.

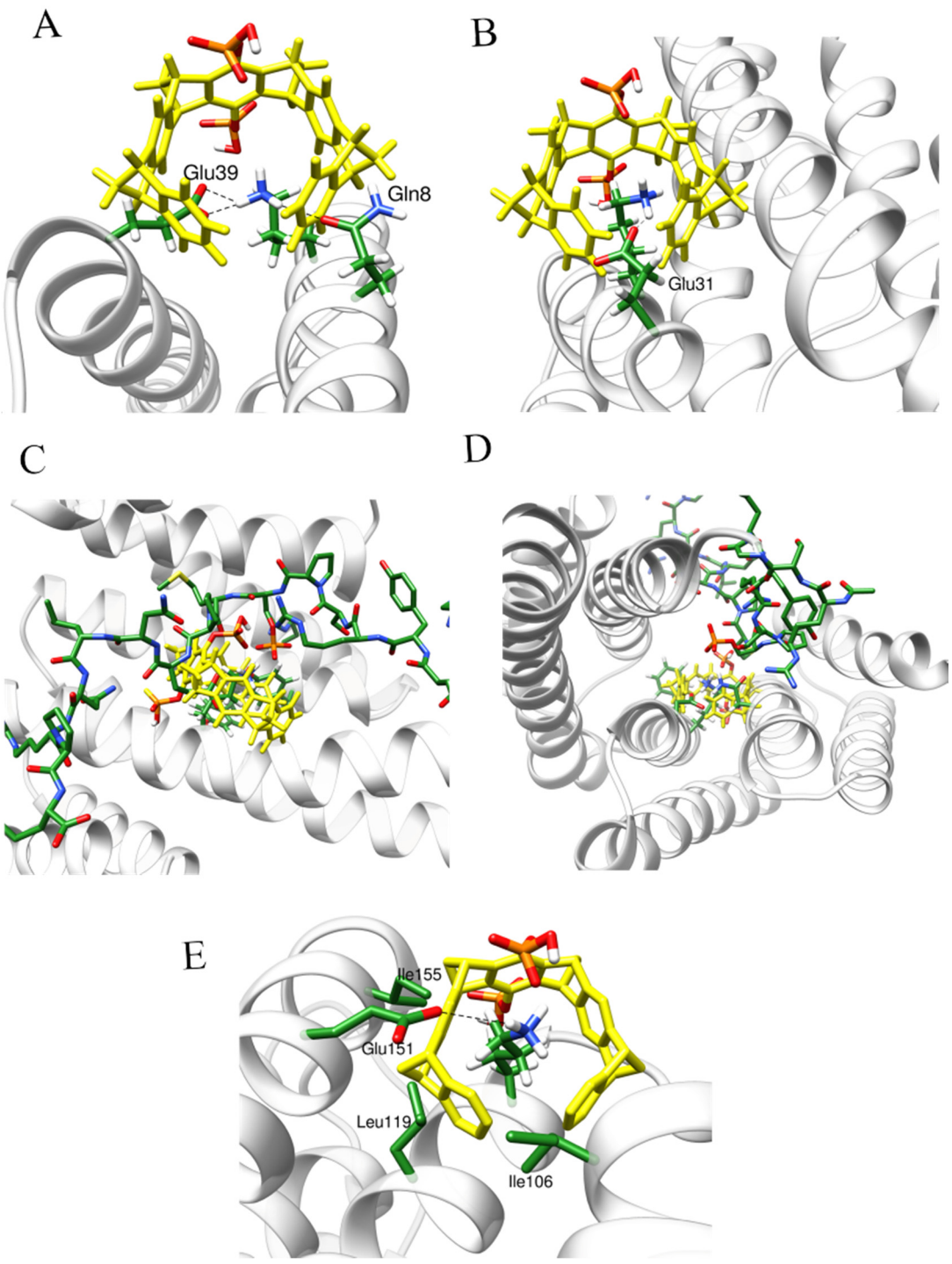

Figure S8. The binding of CLR01 to K11$_{14\text{-}3\text{-}3\zeta}$ (A), K27$_{14\text{-}3\text{-}3\zeta}$ (B), K49$_{14\text{-}3\text{-}3\zeta}$ (C), K120$_{14\text{-}3\text{-}3\zeta}$ (D), and K115$_{14\text{-}3\text{-}3\zeta}$ (E) was sterically disfavored and thus the inclusion complexes were not conserved. The initial structures used for the MD simulations with CLR01 around the corresponding lysine residues are shown.

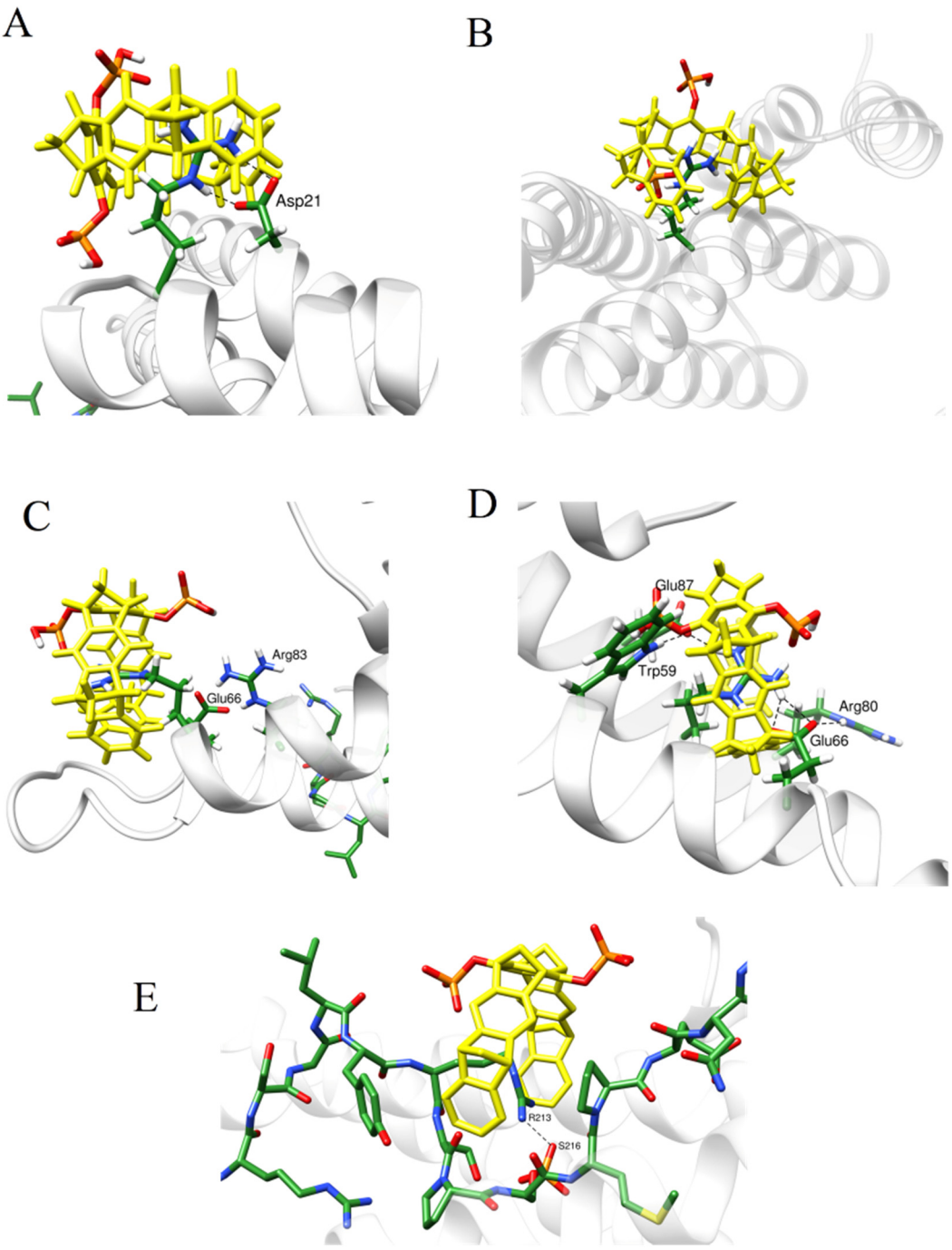

Figure S9. The binding of CLR01 to $R18_{14\text{-}3\text{-}3\zeta}$ (A), $R55_{14\text{-}3\text{-}3\zeta}$ (B), $R80_{14\text{-}3\text{-}3\zeta}$ (C), $R83_{14\text{-}3\text{-}3\zeta}$ (D), and $R213_{Cdc25CpS216}$ (E) was sterically disfavored and thus the inclusion complexes were not conserved. The initial structures used for the MD simulations with CLR01 around the corresponding arginine residues are shown.

Table S2. Average and relative QM energies for the snapshots optimized at the QM/MM level (QM(B3LYP- D3/def2-SVP)/CHARMM27).

	Residue	Average QM energy (hartree)	Relative QM energy (hartree)	Relative QM energy (kcal/mol)
14-3-3ζ LYS-CLR01	K187	-3036.2596	0.00	0 ± 3.6
	K3	-3036.2582	0.0015	0.9±8.7
	K74	-3036.2407	0.0189	11.9 ± 3.2
	K138	-3036.2373	0.0223	14.0 ± 8.4
	K68	-3036.2200	0.0396	24.8 19.4
	K85	-3036.2168	0.0428	26.9 ± 3.1
	K158	-3036.2141	0.0455	28.6 ± 10.1
	K139	-3036.2135	0.0461	28.9 ± 11.7
	K193	-3036.2073	0.0523	32.8 ± 4.6
	K75	-3036.2063	0.0534	33.5 ± 4.0
	K212	-3036.2033	0.0563	35.3 ± 2.9
	K157	-3036.1989	0.0607	38.1 ± 4.2
	K103	-3036.1951	0.0645	40.5 ± 10.2
	K9	-3036.1745	0.0851	53.4 ± 17.2
	K122	-3036.1652	0.0944	59.2 ± 1.9
14-3-3ζ ARG-CLR01	R60	-3145.6801	0.0	0 ± 10.9
	R127	-3145.6607	0.0194	12.2 ± 1.0
	R222	-3145.6219	0.0582	36.5 ± 2.4
	R91	-3145.5891	0.0911	57.1 ± 8.6
	R167	-3145.5464	0.1337	83.9 ± 14.6
	R41	-3145.5097	0.1704	107.0 ± 9.5
	R56	-3145.4570	0.2232	140.0 ± 11.2
Cdc25CpS216	R208	-3145.6941	0.00	0 ± 2.1
ARG-CLR01	R225	-3145.6524	0.0417	26.2 ± 9.6
	R223	-3145.5943	0.0998	62.6 ± 10.3

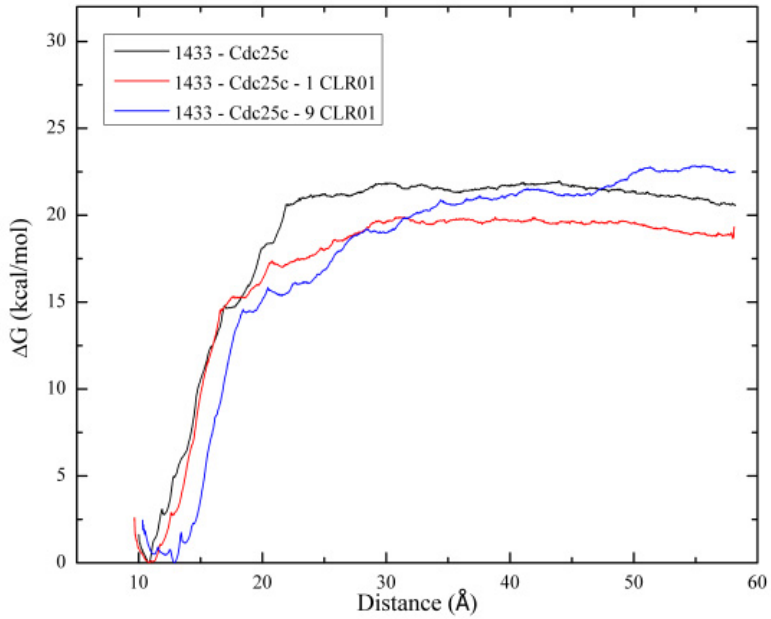
1433 - Cdc25c
1433 - Cdc25c - 1 CLR01
1433 - Cdc25c - 9 CLR01
ΔG (kcal/mol)
Distance (Å)

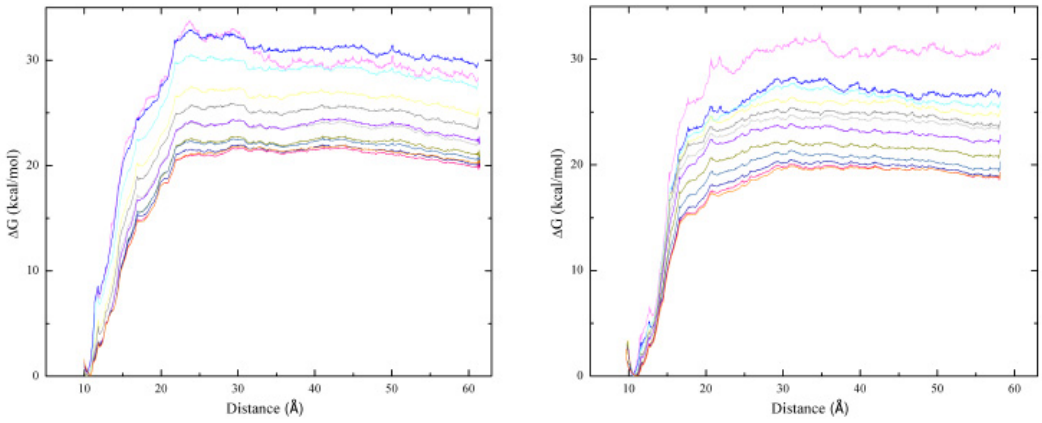
ΔG (kcal/mol)
Distance (Å)

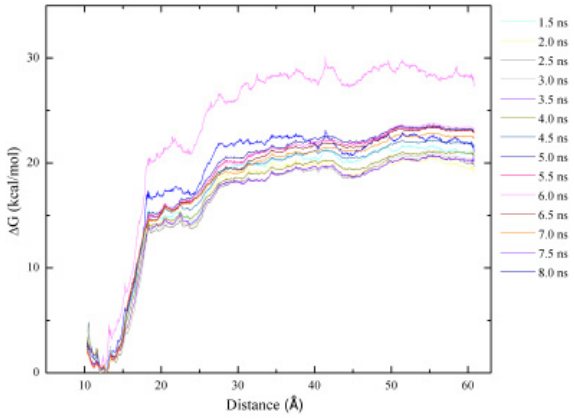
1.5 ns
2.0 ns
2.5 ns
3.0 ns
3.5 ns
4.0 ns
4.5 ns
5.0 ns
5.5 ns
6.0 ns
6.5 ns
7.0 ns
7.5 ns
8.0 ns
ΔG (kcal/mol)
Distance (Å)

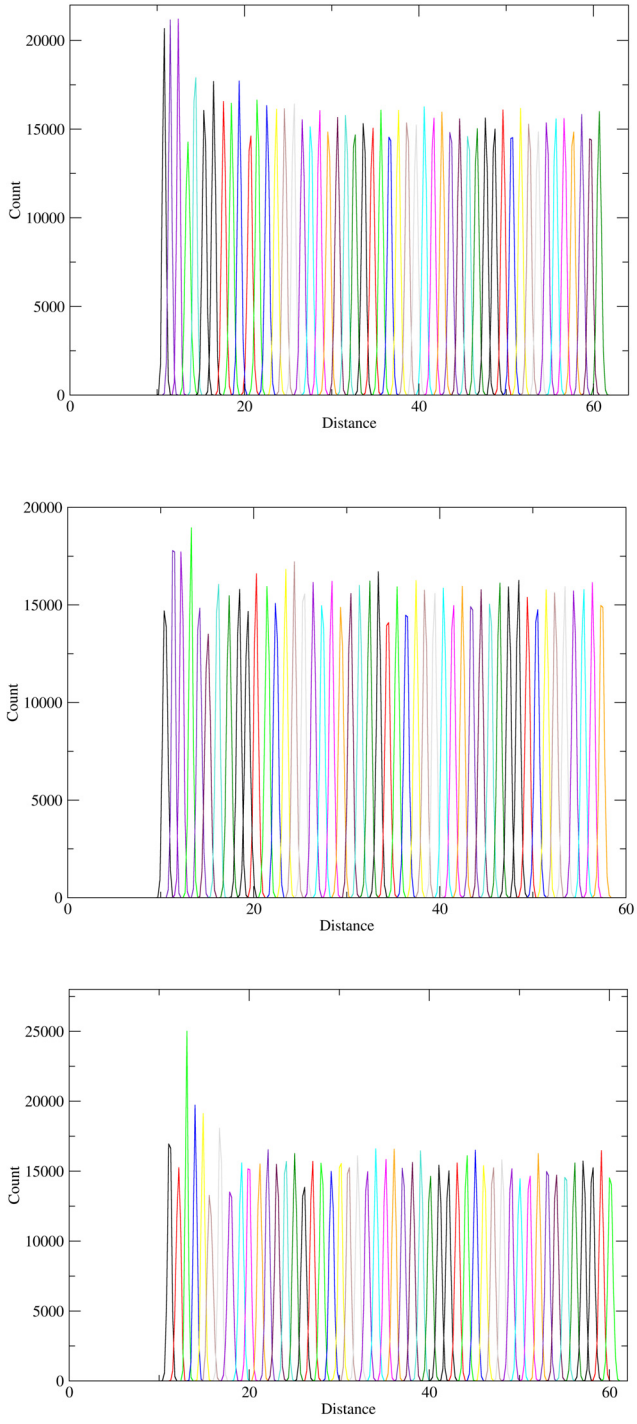

Figure S10. Umbrella sampling calculations. Top: PMF profiles. Middle: Time convergence of all three setups, increasing amount of tweezers, clockwise. Three bottom panels: Window's overlap.

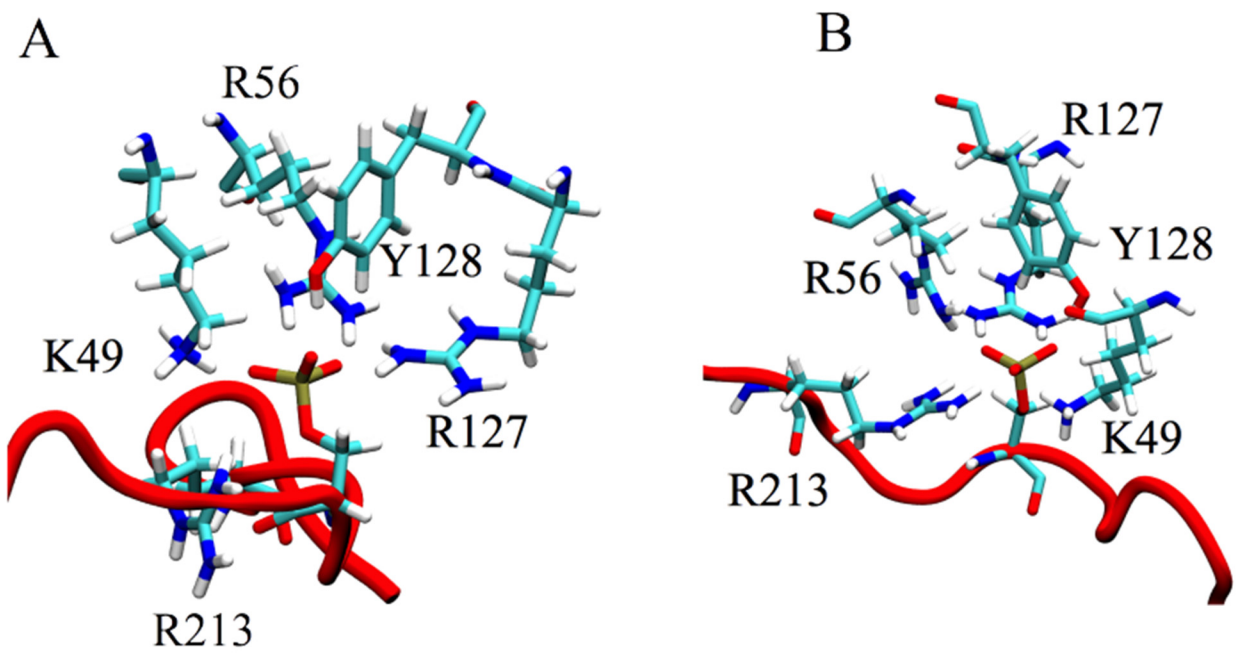

Figure S11. Interaction between R213$_{Cdc25C}$ and S216$_{Cdc25C}$ during the MD simulation of the ternary complex with CLR01 around R208$_{Cdc25C}$. **(A)** Position of R213 at the beginning of the simulation. (**B**) R213$_{Cdc25C}$ interacts with S216$_{Cdc25C}$ during the MD simulation with CLR01. The residues of 14-3-3ζ within 3 Å of S216$_{Cdc25C}$ are shown.

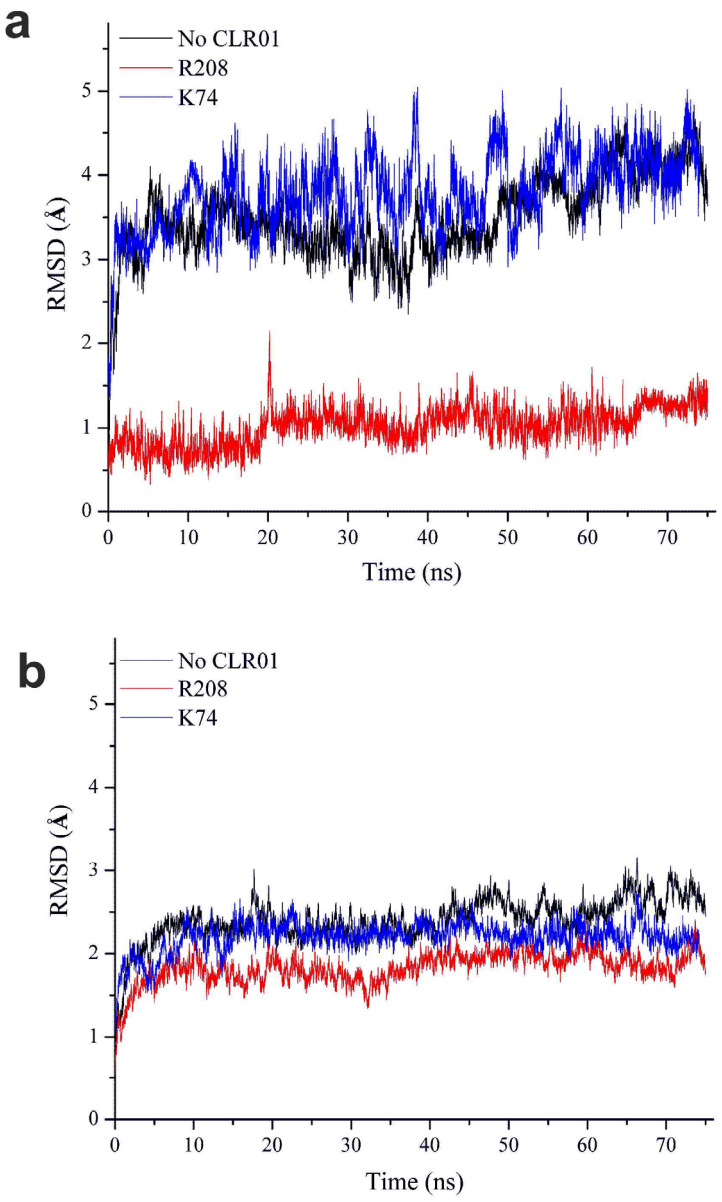

Figure S12. a) The RMSD plots of the **Cdc25CpS216 backbone** during the MD simulations of the 14-3-3ζ – Cdc25CpS216 complex (black), the 14-3-3ζ – Cdc25CpS216 – CLR01$_{K74}$ complex (blue) and the 14-3-3ζ – Cdc25CpS216 – CLR01$_{Arg208}$ complex (red) indicate that the presence of CLR01 on R208 results in a less flexible **peptide.** b) The RMSD plots of the **Cdc25CpS216-14-3-3ζ backbone** during the MD simulations of the 14-3-3ζ – Cdc25CpS216 complex (black), the 14-3-3ζ – Cdc25CpS216 – CLR01$_{K74}$ complex (blue) and the 14-3-3ζ – Cdc25CpS216 – CLR01$_{Arg208}$ complex (red) indicate that the presence of CLR01 on R208 results in a less flexible **peptide-protein complex.** As expected, the overall effect in b) is not as pronounced as in a) since 14-3-3ζ is not a disordered protein.

Other calculations

We also used the model of Janin[21] to evaluate the free energy of dissociation of the 14-3-3 – Cdc25CpS216 complex in the absence and presence of CLR01. The results are shown in Table S3. The PDB entry 1A4O[22] was taken as the reference for the unbound state of 14-3-3ζ. In the case of the unbound Cdc25CpS216 peptide, no crystal or NMR structures are available. Therefore, the contribution of the peptide to the iRMSD term could not be included. Any residue within 4 Å of the peptide was considered as part of the interface.

The values for ΔGd indicate that the stability of the complex increases by 2.5 kcal/mol (38-mer) when CLR01 is added. In addition, the increase in the peptide size from the 20-mer to the 38-mer results in a stability gain of 0.9 kcal/mol when both model peptides are in the presence of the tweezer. These results are in full agreement with the experiments and the free energy calculations discussed in the paper.

However, the values resulting from the application of the Janin model to our system should be treated with caution. We note that, here, we are dealing with a complex system were many aspects regulate the protein-protein interactions, like solvent effects and the addition of the ligand. On the other hand, the approach proposed by Janin is a minimal model of protein-protein affinity based on only two factors: the size of the interface and of the conformational changes between the bond and unbound states. As discussed before, we lack structural information on the unbound Cdc25CpS216 peptide. Importantly, the calculated energy differences lay below the reported error of the Janin approach, which is 4 kcal/mol.

Table S3. Calculated free energies of dissociation using Janin's model

System	ΔASA (Å^2)	iRMSD (Å)	ΔG_d (kcal/mol)
1433 – Cdc25CpS216$_{38mer}$	930.7	0.43	9.3
1433 – Cdc25CpS216$_{20mer}$ – CLR01	1442.1	0.61	10.9
1433 – Cdc25CpS216$_{38mer}$ – CLR01	1650.1	0.60	11.8

References

1 Šali, A. & Blundell. T. L. Comparative protein modelling by satisfaction of spatial restraints. *J. Mol. Biol.* **234**, 779-815 (1993).

2 Brooks, B. R.CHARMM: a program for macromolecular energy, minimization, and dynamics calculations. *J. Comput. Chem*. **4**, 187–217 (1983).

3 MacKerell, A.D. in *Encyclopedia of Computational Chemistry* ed. Schleyer, P. **271** Wiley, Chicester, UK, (1998).

4 Jorgensen, W. L., Chandrasekhar, J., Madura, J. D., Impey, R. W. & Klein, M. L. Comparision of simple potential functions for simulationg liquid water. *J Chem Phys* **79**, 926-935 (1983).

5 Phillips, J.C.; Braun, R.; Wang, W.; Gumbart, J.; Tajkhorshid, E.; Villa, E.; Chipot, C. Skeel RD, Kalé L, Schulten K. Scalable molecular dynamics with NAMD. *J. Comput. Chem.* **26**, 1781–1802 (2005).

6 Mackerell, A. D., Feig, M. & Brooks, C. L., Extending the treatment of backbone energetics in protein force fields: Limitations of gas-phase quantum mechanics in reproducing protein conformational distributions in molecular dynamics simulations. *J. Comput. Chem.* **25**, 1400–1415 (2004).

7 MacKerell, A.D., Bashford, D., Bellott, M., Dunbrack, R.L., Evanseck, J.D., Field, M.J., Fischer, S., Gao, J., Guo, H., Ha, S., Joseph-McCarthy, D., Kuchnir, L., Kuczera, K., Lau, F.T., Mattos, C., Michnick, S., Ngo, T., Nguyen, D.T., Prodhom, B., Reiher, W.E., Roux, B., Schlenkrich, M., Smith, J.C., Stote, R., Straub, J., Watanabe, M., Wiórkiewicz-Kuczera, J., Yin, D., Karplus, M. All-Atom Empirical Potential for Molecular Modeling and Dynamics Studies of Proteins *J. Phys. Chem. B* **102(18)**, 3586-3616 (1998).

8 Andersen, H. C. Rattle: A "velocity" version of the shake algorithm for molecular dynamics calculations. *J. Comput. Phys.* **52 (1)**, 24-34 (1983).

9 Izaguirre, J. A., Catarello, D. P., Wozniakk, J.M. & Skeel, R.D. Langevin stabilization of molecular dynamics. *J. Chem. Phys.* **114 (5)**, 2090-98 (2001).

10 Darden, T. A., York, D. M. & Pedersen L. G. Particle mesh Ewald: An *NlogN* method for Ewald sums in large systems. *J. Chem. Phys.* **98**, 10089–10092 (1998).

11 Sherwood, P.; de Vries, A.H.; Guest, M.F.; Schreckenbach, G.; Lennartz, C. QUASI: A general purpose implementation of the QM/MM approach and its application to problems in catalysis. *J. Mol. Struct. (TEOCHEM)* **632**, 1-28 (2003).

12 Bakowies, D. & Thiel, W. hybrid Models for Combined Quantum Mechanical and Molecular Mechanical approaches. *J. Phys. Chem.* **100**, 10580-10594 (1996).

13. de Vries, A. H. Zeolite Structure and Reactivity by Combined Quantum-Chemical-Classical Calculations. *J. Phys. Chem. B* **103**, 6133-6141 (1999).

14 Antes, I. & Thiel, W. On the treatment of link atoms in hybrid methods. *ACS Symp. Ser.* **712**, 50-65 (1998).

15 Gumbart, J. C., Roux, B., & Chipot, C. Standard binding free energies from computer simulations: What is the best strategy? *J. Chem. Theory. Comput.* **9(1)**, 794–802 (2013).

16 Bennett C. H. Efficient estimation of free energy differences from Monte Carlo data. *J. Chem. Phys.* **22**, 245–268 (1976).

17 Liu, P., Dehez, F., Cai, W. & Chipot, C. A toolkit for the analysis of free-energy perturbation calculations, *J. Chem. Theor. Comput.* **8**, 2606-2616 (2012).

18 Torrie, G. M. & Valleau, J. P. Nonphysical Sampling Distributions in Monte Carlo Free-Energy Estimation: Umbrella Sampling. *J. Comput. Phys.* **23**, 187–199 (1977).

19 Xiaowen Y., Wen H. L., Sobott F., Papagrigoriou E., Robinson C. V., Grossmann J. G., Sundström M., Doyle D. A. & Elkins J. M. Structural basis for protein–protein interactions in the 14-3-3 protein family. *PNAS* **103**(46), 17237-17242 (2006)

20. Wang, H., L. Zhang, R. Liddington, & H. Fu. Mutations in the hydrophobic surface of an amphipathic groove of 14-3-3ζ disrupt its interaction with Raf-1 kinase. *J. Biol. Chem.* **273**, 16297-16304 (1998).

21. Janin, J. A minimal model of protein–protein binding affinities. *Protein Sci.* **23**, 1813 (2014).

22. Liu, D.; Bienkowska, J.; Petosa, C.; Collier, R. J.; Fu, H.; Liddington, R. Crystal structure of the zeta isoform of the 14-3-3 protein. *Nature* **376**, 191 (1995).